frontiers | Frontiers in Molecular Biosciences

TYPE Original Research
PUBLISHED 13 January 2025
DOI 10.3389/fmolb.2024.1529027

OPEN ACCESS

EDITED BY
Vânia Vilas-Boas,
International Iberian Nanotechnology Laboratory (INL), Portugal

REVIEWED BY
Elisa De Luca,
National Research Council (CNR), Italy
Laure-Alix Clerbaux,
UCLouvain, Belgium

*CORRESPONDENCE
Mattia Santoni,
mattia.santoni@unibo.it

†These authors have contributed equally to this work and share first authorship

‡These authors have contributed equally to this work and share last authorship

RECEIVED 15 November 2024
ACCEPTED 19 December 2024
PUBLISHED 13 January 2025

CITATION
Santoni M, Piccinini G, Liguori G, Randi MR, Baroncini M, Milani L and Danesi F (2025) Enhanced intestinal epithelial co-culture model with orbital mechanical stimulation: a proof-of-concept application in food nanotoxicology.
Front. Mol. Biosci. 11:1529027.
doi: 10.3389/fmolb.2024.1529027

Enhanced intestinal epithelial co-culture model with orbital mechanical stimulation: a proof-of-concept application in food nanotoxicology

Mattia Santoni[1*†], Giovanni Piccinini[1,2†], Giovanni Liguori[2], Maria Roberta Randi[2], Massimo Baroncini[1‡], Liliana Milani[2‡] and Francesca Danesi[1‡]

[1]Department of Agricultural and Food Sciences (DISTAL), University of Bologna, Cesena, Italy, [2]Department of Biological, Geological, and Environmental Sciences (BiGeA), University of Bologna, Bologna, Italy

Introduction: Current *in vitro* intestinal models lack the mechanical forces present in the physiological environment, limiting their reliability for nanotoxicology studies. Here, we developed an enhanced Caco-2/HT29-MTX-E12 co-culture model incorporating orbital mechanical stimulation to better replicate intestinal conditions and investigate nanoparticle interactions.

Methods: We established co-cultures under static and dynamic conditions, evaluating their development through multiple approaches including barrier integrity measurements, gene expression analysis, and confocal microscopy. We introduced novel quantitative analysis of dome formation as a differentiation marker and demonstrated the model application by investigating cellular responses to titanium dioxide (TiO_2) nanoparticles in a digested food matrix.

Results: Dynamic conditions accelerated epithelial differentiation, achieving functional barrier properties by day 14 rather than day 21, with enhanced mucin production and more organized three-dimensional structure. Mechanical stimulation selectively promoted goblet cell differentiation without affecting general epithelial markers. The optimized model successfully detected concentration-dependent oxidative stress responses to TiO_2 exposure, revealing cellular dysfunction preceding membrane damage.

Discussion: This improved co-culture system provides a better physiological platform for nanotoxicology studies. By incorporating mechanical forces, each cell type exhibits more representative behavior, creating a more realistic experimental setup. The model bridges the gap between simple monocultures and complex 3D systems, offering a practical

approach for investigating nanoparticle-epithelium interactions in a food-relevant context.

KEYWORDS

dome formation, epithelial differentiation, *in vitro* digestion, intestinal barrier model, mechanical stimulation, nanotoxicology, oxidative stress, titanium dioxide nanoparticles

1 Introduction

The human intestinal epithelium functions as a critical interface between the body and external environment, maintaining selective barrier properties while facilitating nutrient absorption and immune modulation. Understanding epithelial barrier function and regulation requires physiologically relevant *in vitro* models. While Caco-2 monocultures have been widely used due to their ability to differentiate into enterocyte-like cells with functional tight junctions and brush border microvilli (Basson et al., 1998; Sambuy et al., 2005), they lack the cellular heterogeneity of the intestinal epithelium (Pereira et al., 2016), particularly a functional mucus layer essential for barrier protection and immune regulation (Song et al., 2023).

Co-culture systems combining Caco-2 cells with mucus-producing HT29-MTX cells better replicate intestinal conditions. The HT29-MTX-E12 subclone exhibits enhanced goblet cell differentiation and mucus secretion (Lesuffleur et al., 1993; Behrens et al., 2001), providing a more physiologically relevant model for studying gut permeability, nanoparticle interactions, and responses to pro-oxidative or pro-inflammatory agents (Antunes et al., 2013; Martínez-Maqueda et al., 2015; Johansson and Hansson, 2016). However, achieving optimal differentiation in these co-culture systems remains challenging, requiring precise optimization of both biochemical stimuli—such as dexamethasone and butyrate (Liang et al., 2000; Willemsen et al., 2003)—and mechanical factors (Frohlich and Roblegg, 2012).

Traditional static culture conditions fail to replicate the physical forces—such as fluid shear stress and cyclic strain—present in the intestinal environment. These mechanical forces are essential for proper epithelial polarization and barrier function (Liu et al., 2022). While dynamic culture systems incorporating controlled mechanical stimulation show promise, their effects on differentiation timing and barrier development remain incompletely characterized. Additionally, established markers of epithelial differentiation like brush border enzyme expression and barrier integrity measurements may not fully capture the complexity of mechanical force-induced changes.

Dome formation—the development of fluid-filled, three-dimensional structures reflecting active ion transport beneath polarized monolayers—represents a promising but underutilized marker of epithelial differentiation (Lechner et al., 2011). These structures indicate functional barrier properties and polarized organization (Lever, 1985; Bohets et al., 2001), resembling the natural architecture of intestinal epithelium. Dome formation typically begins 5–8 days post-confluence, with structures increasing in size and density through fusion events (Hara et al., 1993). These regions exhibit specialized transport functions and increased brush border enzyme expression (Matsumoto et al., 1990; Ferraretto et al., 2007), making dome quantification valuable for assessing differentiation kinetics (Zweibaum et al., 2011). Advanced imaging technologies, particularly confocal microscopy, now enable detailed analysis of dome formation dynamics (Rotoli et al., 2002), potentially providing new insights into differentiation processes. While 3D models like organoids offer improved physiological relevance, their complexity and cost limit widespread application, making optimized 2D co-culture systems a practical alternative (Baptista et al., 2022).

In this study, we introduce an enhanced co-culture model incorporating orbital mechanical stimulation to accelerate differentiation. We establish dome formation as a quantitative marker of differentiation state, employing confocal microscopy and computational image analysis to characterize three-dimensional epithelial organization. Beyond testing the model's potential, we also explore its application for studying epithelial cell interactions with food components by supplementing the model with *in vitro* semi-dynamic digested test food containing 1% w/v titanium dioxide (TiO_2) nanoparticles. TiO_2 is a common whitening agent employed as food additive (E171) (Weir et al., 2012; Peters et al., 2014; Rompelberg et al., 2016; Ropers et al., 2017). While TiO_2 is currently approved by the Food and Drugs Administration (FDA) as safe for use in foods up to 1% by weight (FDA, 2024), a position recently reaffirmed by the Joint FAO/WHO Expert Committee on Food Additives (JECFA, 2023), research has shown that TiO_2 food additive contain particles in the nanoscale range (<100 nm) that can accumulate in intestinal tissues. These nanoparticles have been associated with adverse effects including genotoxicity and oxidative stress in both *in vitro* studies (Koeneman et al., 2009; Gerloff et al., 2012; McCracken et al., 2013; Dorier et al., 2015; Cao et al., 2020), pre-clinical mouse models (Wang et al., 2007; Bettini et al., 2017), and humans (Heringa et al., 2018). Based on these concerns the European Food Safety Authority (EFSA) concluded that E171 could no longer be considered safe as a food additive (EFSA Panel on Food Additives and Flavourings et al., 2021; Boutillier et al., 2022).

Our objectives were to: (1) develop and test an enhanced differentiation protocol using orbital mechanical stimulation, (2) establish quantitative analysis methods for dome formation as a differentiation marker, and (3) demonstrate the model's application by investigating epithelial responses to TiO_2 nanoparticles in the context of an *in vitro* digested food matrix. This optimized system bridges the gap between simple monocultures and complex 3D models, providing a robust platform for investigating intestinal barrier function, nutrient and drug absorption, while contributing to a growing field of research on nanoparticle interactions with the gut epithelium.

2 Materials and methods

2.1 Materials

All materials used in this study were obtained from Sigma-Aldrich (St. Louis, MO, United States) or Merck (Darmstadt, Germany) unless otherwise specified.

2.2 Development of enhanced Caco-2/HT29-MTX-E12 co-culture

2.2.1 Cell culture establishment and maintenance

Caco-2 cells and HT29-MTX-E12 cells (ECACC; Porton Down, UK) were maintained in complete Dulbecco's Modified Eagle Medium (DMEM; Gibco, Waltham, MA, United States). The medium was supplemented with 10% fetal bovine serum (FBS), 1% non-essential amino acids (NEAA; Gibco, Waltham, MA, United States), 1% GlutaMAX™ (Gibco), and 1% penicillin-streptomycin (Gibco). Both cell lines were cultured at 37°C in a humidified atmosphere containing 5% CO_2, with media changes performed every 48 h.

For co-culture establishment, both cell lines were independently cultured until reaching 80% confluence, after which they were harvested using 0.25% trypsin-EDTA solution. Cell viability and counts were determined using the Trypan Blue exclusion assay (Bio-Rad Laboratories, Hercules, CA, United States) on a TC20 Automated Cell Counter (Bio-Rad Laboratories). Subsequently, the cells were seeded in a physiologically relevant ratio of 9:1 (Caco-2:HT29-MTX-E12), representing the approximate proportion of enterocytes to goblet cells found in the human small intestinal epithelium (Welcome, 2018; Paone and Cani, 2020). The cell mixture was seeded onto Transwell® permeable supports (pore size: 0.4 µm, surface area: 1.12 cm^2; Corning, New York, NY, United States) at a density of 1×10^5 cells/cm^2 in 12-well cell culture multiwell plates (Corning). Co-cultures were maintained in complete DMEM with media changes every 48 h throughout the experimental period.

2.2.2 Static and dynamic culture conditions for cell differentiation

Following seeding, co-cultures were initially maintained under static conditions until reaching confluence (approximately 7 days, designated as T0). Post-confluence, cultures were divided into two experimental groups:

(i) Static condition: co-cultures were maintained in a standard cell culture incubator without mechanical stimulation.

(ii) Dynamic condition: co-cultures were placed on a Celltron orbital shaker (Infors HT, Basel, Switzerland) set to 55 rpm, housed within a cell culture incubator. The shaker's orbital diameter of 25 mm generated an estimated fluid shear stress of 0.17 Pa (1.7 dynes/cm^2) at the cell surface [calculated according to Dardik et al. (2005)]. This value falls within the physiological range, representing moderate-high fluid shear stress, as intestinal cells experience shear forces of 1–5 dynes/cm^2 during digestion, attenuated to <1 dyne/cm^2 by the microvilli barrier (Guo et al., 2000).

Both conditions were maintained at 37°C with 5% CO_2 throughout the 21-day differentiation period. Media was changed every 48 h, with care taken to maintain identical handling procedures between static and dynamic conditions except for the orbital motion.

2.3 Characterization of the co-culture model

The development and functional differentiation of the co-culture model were assessed through multiple complementary approaches, including barrier function, molecular markers, morphological analysis, and imaging techniques.

2.3.1 Functional assessment

The co-culture model's functional properties were evaluated by measuring barrier integrity, permeability, gene expression of differentiation markers, and mucin production.

2.3.1.1 Transepithelial electrical resistance (TEER) measurement

The integrity of the barrier in the Caco-2/HT29-MTX-E12 co-cultures was monitored by measuring transepithelial electrical resistance (TEER) every other day during the 21-day differentiation period. TEER measurements were performed under sterile conditions using a Millicell ERS-2 Voltohmmeter (Millipore, Burlington, MA, United States). The culture medium was replaced before each TEER measurement, and the culture was equilibrated for 30 min at 37°C and 5% CO_2. Prior to each use, the electrode was sterilized with 70% ethanol and air-dried for 10 min. To maintain optimal cell conditions during measurement, the culture plate was placed on a temperature-controlled heating block (StableTemp Dry Block Heater, Cole-Parmer; Vernon Hills, IL, United States) set to 37°C. TEER values were corrected by subtracting the resistance of a cell-free Transwell insert, and final TEER values were normalized to the surface area of the insert. For each condition, three independent co-cultures were established, with each time point representing the average value across replicates.

2.3.1.2 Paracellular permeability assessment

Paracellular permeability was assessed by measuring the transepithelial transport of phenol red (phenolsulfonphthalein), which was selected as a low molecular weight marker (376 Da) allowing detection of changes in tight junction integrity and barrier formation (Smetanová et al., 2011). Following protocols adapted from Ferruzza et al. (2003) and Jiang et al. (2013), the co-cultures were rinsed with pre-warmed Receiving Buffer (RB), composed of Hank's Balanced Salt Solution (HBSS; Gibco) supplemented with 11 mM glucose and 25 mM HEPES (4-(2-hydroxyethyl)-1-piperazineethanesulfonic acid) pH 7.4 (Lonza, Basel, Switzerland). The apical (AP) compartment received 0.5 mL of Donor Buffer (DB: HBSS containing 1 mM phenol red, 11 mM glucose, and 25 mM HEPES, pH 7.4), while 1.5 mL of RB was added to the basolateral (BL) compartment. Samples (100 µL) were collected from the BL compartment at 20-minute intervals over 3 h, with equivalent volumes of fresh RB added to maintain constant volume. The phenol red concentration in BL samples

was quantified spectrophotometrically at 479 nm. Transepithelial flux was expressed as the apparent permeability coefficient (P_{app}), calculated using the equation from Jiang et al. (2013):

$$P_{app} = K \times Vr \times A^{-1}$$

where K represents the steady-state rate of change in phenol red concentration over time in the BL compartment (s^{-1}), Vr is the volume of the receiver chamber (1.5 mL), and A is the surface area of the membrane (1.12 cm^2). The Area Under the Curve (AUC) was calculated for each differentiation time point to quantify and represent the co-culture permeability over time.

2.3.1.3 Gene expression analysis of intestinal differentiation markers

RNA was isolated from co-cultures at four time points (T0, T1, T2, and T3; days 0, 7, 14, and 21, respectively). Cells were washed twice with 1 mL warm Dulbecco's Phosphate-Buffered Saline (DPBS), scraped in 1 mL cold DPBS, and collected by centrifugation at 250 × g for 5 min at 4°C. Cell pellets were lysed in 300 µL TRI Reagent (Zymo Research; Orange, CA, United States) and stored at −80°C until processing. Total RNA was extracted using the Direct-zol RNA MiniPrep kit (Zymo Research) following manufacturer's protocol with modifications. Cell lysis was enhanced using a Bioruptor sonicator (Diagenode; Denville, NJ, United States) for three cycles (30 s ON/30 s OFF) at 4°C with high power settings. Lysates were centrifuged at 845 × g for 5 min at room temperature. RNA quality and quantity were assessed using a NanoDrop ND-2000 spectrophotometer (Thermo Fisher Scientific; Wilmington, DE, United States), with acceptable quality indicated by 260/280 ratios of approximately 2.0–2.1 and 260/230 ratios between 2.0 and 2.2.

cDNA synthesis was performed using 2 µg total RNA with the High-Capacity RNA-to-cDNA Kit (Applied Biosystems; Foster City, CA, United States). Quantitative PCR (qPCR) was conducted using a CFX Connect Real-Time PCR Detection System (Bio-Rad Laboratories) with TaqMan Fast Advanced Master Mix (Applied Biosystems). The thermal cycler conditions were as follows: uracil-N glycosylase incubation at 50°C for 2 min and polymerase activation at 95°C for 20 s, followed by 40 cycles of denaturation at 95°C for 3 s and annealing/extension at 60°C for 30 s. The target genes were selected to assess key intestinal functions, including those encoding tight junction proteins [*CDH1* (cadherin-1) and *TJP1* (zonula occludens-1)], intestinal brush border enzymes [*ALPI* (intestinal alkaline phosphatase), *DPP4* (dipeptidyl peptidase-4), *SI* (sucrase-isomaltase)], and mucin glycoproteins [*MUC2* (mucin-2) and *MUC5AC* (mucin-5AC)]. All TaqMan probe sets used in this study were purchased from Applied Biosystems (Supplementary Table S1). Among four candidate reference genes (*ACTB*, actin beta; *GAPDH*, glyceraldehyde-3-phosphate dehydrogenase; *PPIA*, peptidylprolyl isomerase A; *RPLP0*, ribosomal protein lateral stalk subunit P0), *GAPDH* and *RPLP0* genes were identified as the most stable reference genes, with M values <0.5, and used to normalize the expression of the target genes using the ΔCt method. Target gene expression was normalized to the geometric mean of these two reference genes (Vandesompele et al., 2002). Samples were analyzed in duplicate, with replicates showing cycle threshold (Ct) differences greater than 0.25 being reanalyzed. Data were processed using Bio-Rad CFX Maestro 2.3 Version 5.3.

2.3.1.4 Mucin quantification

Intracellular mucins were quantified using a modified periodic acid-Schiff (PAS) assay based on the methods of Mantle and Allen (1978), with modifications from Yamabayashi (1987) and Miner-Williams et al. (2009). The PAS method was selected for its specificity in quantifying glycoprotein content through reaction with 1,2-glycol groups (Dharmani et al., 2009; Harrop et al., 2012), allowing reliable detection even at low concentrations (Kilcoyne et al., 2011). Briefly, total soluble proteins were extracted from cell cultures using RIPA buffer, following manufacturer's instructions. The samples were centrifuged at 2,000 × g for 10 min, and the supernatant was diluted 1:5 in DPBS. A standard curve was prepared using porcine stomach mucin (10–1,500 µg/mL). Both samples and standards underwent oxidation with periodic acid at 37°C for 2 h, followed by staining with Schiff's reagent for 30 min at room temperature. Absorbance measurements were performed at 550 nm using an Infinite M200 microplate reader (Tecan; Männeford, Switzerland). Mucin concentrations were determined based on the standard curve.

2.3.2 Morphological assessment

To visualize the morphology of the co-cultures, the presence of the mucus layer, and formation of domes, Caco-2/HT29-MTX-E12 cells grown on the Transwell permeable supports under static and dynamic conditions were examined at post-confluence by confocal microscopy at days 0, 7, 14, and 21 (T0, T1, T2, T3, respectively).

The co-cultures were incubated with fluorescent wheat germ agglutinin (WGA Oregon Green® 488 Conjugate; Ex 496 nm, Em 524 nm) (Thermo Fisher Scientific) at a concentration of 5 µg/mL for 20 min in cell culture conditions (37°C and 5% CO_2). WGA specifically binds sialic acid and N-acetylglucosaminyl residues, which are predominant in mucins (Kilcoyne et al., 2011), thus used for mucus layer visualization. Then, co-cultures were fixed with 4% formaldehyde (in DPBS) for 15 min at 37°C and then washed multiple times with DPBS. To stain nuclei, fixed cells were incubated with TO-PRO-3 iodide (Ex 642 nm, Em 661 nm) (Thermo Fisher Scientific) at a 1:2000 dilution in DPBS for 10 min at room temperature. After staining, the co-cultures were washed multiple times with DPBS. For microscopy preparation, the Transwell membranes were carefully excised from their plastic inserts using a scalpel by inserting the blade from the underside of the membrane and cutting around the perimeter, following an adaptation of protocol by Hiebl et al. (2020). The membranes were then gently lifted using fine forceps, gripping only the circular edges to preserve the cell layer integrity. The excised membranes were mounted on glass slides using anti-fade medium [2.5% 1,4-diazabicyclo [2.2.2] octane (DABCO), 50 mM Tris, pH 8, and 90% glycerol], taking special care to avoid air bubbles and maintain proper orientation for subsequent microscopic analysis.

2.3.2.1 Confocal microscopy analysis

Images were acquired with a Nikon A1R + HD25 confocal laser scanning microscope with a 60 × oil immersion objective (NA 1.4). To capture a large area at high resolution, we employed the Large Image function of the Nikon software (Nis-Elements AR 5.20). This function created composite images by automatically

assembling 6 × 6 individual image fields into larger mosaic images. The tile scanning was performed across multiple z-planes to generate comprehensive 3D mosaics of adjacent image stacks. Z-stack images were acquired (Schindelin et al., 2012), with three areas of ~1 mm^2 imaged from the central region of the Transwell membrane for each time point sample (T0, T1, T2, T3) and for each of the two treatments (static and dynamic condition). Images were acquired at 2 µm intervals, starting from the Transwell membrane on which the cells were grown to the top of the cell multi-layer, and numbered in ascending order. The appearance of the mucus layer that covers the cultures was indeed taken as an indication of cell top reaching. In this way, each image corresponded along z to the image with the same number in other samples (*e.g.*, image #4 of all the samples had the same height, that is at ~8 µm of height, from the membrane surface). The confocal microscopy imaging allowed for the analyses of the overall morphology of the co-cultures, including cell distribution and dome formation. The continuity of the mucus layer was evaluated by examining the WGA staining in the z-stack images.

2.3.2.2 Image processing and analysis

Post-acquisition image processing and dome formation analysis were conducted using ImageJ Fiji (v1.54f). Confocal image stacks were imported using the Bio-Formats plugin in hyperstack format, which enabled accurate handling of metadata and preserved multidimensional data integrity. For three-dimensional visualization, surface topography was reconstructed using the "3D Surface Plot" plugin, with parameters optimized for dome structure analysis. These included a grid size of 128 to achieve optimal spatial resolution, "Filled Gradient" appearance settings to enhance surface continuity visualization, and a Z-scale factor of 0.1 to maintain proportional spatial representation.

For detailed dome formation analysis, each section from the stacked images was exported individually as a composite file containing merged channels. To ensure data quality, sections containing glass slide grid artifacts were excluded from the analysis. Areas with weak green signal representing cellular presence were selectively enhanced in Adobe Photoshop 2024 (Adobe Inc., San Jose, CA, United States) to improve visualization clarity while maintaining signal fidelity.

2.3.2.3 Quantitative and qualitative assessment of domes

Dome formations in 3D reconstructed images were detected and quantified using Python with the OpenCV library, along with additional image processing packages (scikit-image, SciPy, and Matplotlib). Each image was analyzed from four different angle views to enhance detection accuracy. The images were first normalized to a 0–1 intensity range, followed by conversion to grayscale and adaptive segmentation to isolate dome-like structures. Each detected region was further characterized by measuring its area and height, though these detailed measurements were not included in the final analysis (data not shown).

Each composite image was analyzed using Python's Open-Source Computer Vision Library (OpenCV). Specifically, after binarizing each image, contiguous cell-covered objects were identified and characterized by two parameters: area extension (measured in pixels) and eccentricity (ranging from 0 to 1). The eccentricity parameter reflects the shape's elongation, calculated as the ratio of the distance between the foci of an ellipse (fit to each contour) to its major axis length, with values closer to 0 indicating circular shapes and values near 1 indicating highly elongated shapes.

2.4 Assessment of co-culture model with food components

To evaluate the enhanced co-culture model's utility for food safety assessment, we first evaluated its biocompatibility with digested skimmed milk powder (SMP) (SaporePuro; Gioia Group, Torino, Italy), as test food matrix, followed by investigating cellular responses to SMP supplemented with TiO_2 nanoparticles.

2.4.1 Digestion and supplementation of SMP with TiO_2 nanoparticles

2.4.1.1 Semi-dynamic *in vitro* digestion of SMP

A semi-dynamic *in vitro* digestion protocol was performed on 10% w/v SMP solution (10 g SMP dissolved in 100 mL distilled water) following the standardized INFOGEST method (Mulet-Cabero et al., 2020) with bio-compatibility modifications. The process began with an oral phase where 30 mL of SMP solution was combined with 10 mL simulated salivary fluid (SSF) without amylase (since the food matrix contained no starch; Supplementary Table S2) and maintained at 37°C with constant stirring for 2 min. For the gastric phase, the oral bolus was mixed with simulated gastric fluid (SGF) containing porcine pepsin (2,000 U/mL, Sigma-Aldrich). To simulate physiological gastric emptying, an automated titrator (Metrohm, Herisau, Switzerland) gradually reduced the pH to 3.0 over 60 min, with emptying events occurring every 20 min. The intestinal phase commenced with the addition of simulated intestinal fluid (SIF) containing porcine pancreatin (100 U/mL, Sigma-Aldrich), maintaining pH 7.0 for 120 min at 37°C under continuous stirring in a climate-controlled hood (Model 810; ASAL s.r.l., Cernusco sul Naviglio, Italy) equipped with an orbital shaker (Model 709; ASAL s.r.l.). Bile was omitted from the intestinal phase since previous studies showed they are a major source of cytotoxicity in cell experiments (Vieira et al., 2022). Additionally, the SMP used contained relatively low lipid content (Supplementary Table S2), reducing its need in the digestion process (Atallah et al., 2020). Three independent digestions were performed. After pooling the samples, they were immediately frozen in liquid nitrogen to halt enzymatic activity (Kondrashina et al., 2024). After rapid thawing, the samples were processed to obtain the bioaccessible fraction. First, to obtain a clear supernatant, samples were centrifuged (10,000 × g, 30 min, 4°C) and filtered through a 0.45 µm polyethersulfone (PES) membrane (Millipore). Then, the filtrate was ultrafiltered using a 3 kDa Vivaspin® 20 centrifugal filter (Sartorius AG, Göttingen, Germany) to remove larger proteins and enzymes (Giromini et al., 2019), and finally sterilized through a 0.22 µm PES membrane (Millipore) (Segeritz and Vallier, 2017).

2.4.1.2 TiO_2 solubilization in digested SMP

TiO_2 effect on epithelial cells was investigated by incorporating anatase TiO_2 nanoparticles (−325 mesh, catalog #248576) into the

digested SMP bioaccessible fraction (Faria et al., 2020). Following a modified Nanogenotox dispersion protocol (Jensen et al., 2011), TiO_2 was pre-wetted with 0.05% ethanol, centrifuged (3,000 × g, 1 min), and the pellet was resuspended in digested SMP to achieve 0.25% TiO_2 concentration. This concentration accounts for the 1:8 dilution factor inherent to the digestion protocol while maintaining equivalence to the FDA-permitted maximum of 1% w/v TiO_2 in the original food matrix (FDA, 2024). The suspension underwent 32 sonication cycles (30 s each) followed by 0.22 µm PES membrane filtration to ensure complete dispersion and sterility.

2.4.1.3 Titanium quantification

Titanium content in digesta samples was determined using Inductively Coupled Plasma Optical Emission Spectrometry (ICP-OES, Spectro Arcos-Ametek, Kleve, Germany). The instrument was equipped with an axial torch and high salinity kit. Analysis was performed in duplicate with 12-second measurement runs, each preceded by a 60-second stabilization period. Quantification was achieved using a calibration curve constructed with certified aqueous titanium standards, with a limit of detection (LOD) of 0.33 ppb.

2.4.2 Impact of TiO_2-supplemented SMP digesta on co-culture model

The potential cytotoxicity and oxidative stress effects of TiO_2-supplemented digesta were evaluated through multiple complementary assays examining cell viability, membrane integrity, and redox status markers in the co-culture model. Results in the treated cells were compared to control cells receiving only serum- and phenol red-free DMEM and otherwise handled identically to treated cells.

2.4.2.1 Cell viability assessment

The bioaccessible fraction of digested SMP (with and without TiO_2) was prepared for cell exposure by dilution in serum- and phenol red-free DMEM. Non-spiked digesta was diluted at 1:3, 1:10, and 1:20 (v/v) ratios, while TiO_2-spiked digesta was diluted at 1:3 and 1:10 based on results reported in section 3.3. Cell viability was assessed using PrestoBlue Cell Viability Reagent (PB, Thermo Fisher Scientific, 1:10 dilution). Differentiated co-cultures (21 days, dynamic conditions) were exposed apically to 0.5 mL of diluted digesta for 3 h at 37°C, approximating physiological intestinal transit time (Hardy et al., 1989). Control cells received serum-free DMEM with 1:10 PB. Fluorescence measurements (excitation: 560 nm, emission: 590 nm) were performed using an Infinite F200 microplate reader (Tecan), with blank correction (PB in serum-free DMEM). Cell viability was expressed as the percentage of blank-corrected fluorescence of SMP digesta-exposed cells relative to blank-corrected fluorescence of control cells.

2.4.2.2 Membrane integrity assessment

Cell membrane integrity was evaluated by measuring lactate dehydrogenase (LDH) release from the cytoplasm into the culture medium (phenol red-free DMEM) using the CyQUANT LDH Cytotoxicity Assay Kit (Invitrogen). Absorbance was measured at 490 nm with background correction at 680 nm (Infinite M200, Tecan). LDH release was expressed as a percentage of maximum LDH activity (obtained from lysed control cells).

2.4.2.3 Evaluation of oxidative status and antioxidant defense markers

Multiple parameters were assessed to characterize cellular oxidative status. For lipid peroxidation assessment, thiobarbituric acid reactive substances (TBARS) levels were quantified in culture media (phenol red-free DMEM) following Potter et al. (2011). Media samples (500 µL) were combined with 400 µL of 15% trichloroacetic acid (TCA) and 800 µL of thiobarbituric acid (TBA) solution [0.67% TBA, 0.01% butylated hydroxytoluene (BHT)]. After heating (95°C, 20 min) and cooling, the organic phase was extracted with 3 mL butanol. The upper phase (200 µL) was analyzed for fluorescence, with TBARS expressed as malondialdehyde (MDA) equivalents using a standard curve (0.007–4 nmol/mL).

For glutathione status determination and ROS measurements, treated and control cells were lysed with RIPA buffer following manufacturer's instructions to extract total soluble proteins, which were quantified using Quick Start™ Bradford Protein Assay (Bio-Rad Laboratories). For GSH and GSSG were measured using a modified Ellman's method (Vuolo et al., 2022). Samples were deproteinated (3 volumes 5% TCA, 12,000 × g, 5 min, 4°C) and analyzed in a 96-well format. For GSH measurement, 50 µL sample or standard (0–500 nmol/mL) was combined with 50 µL Tris/EDTA buffer (1 mM Tris, 2 mM EDTA, pH 8.2) and 20 µL 5,5′-dithiobis (2-nitrobenzoic acid) (DTNB, 10 mmol/L). After dark incubation (15 min, room temperature), absorbance was measured at 412 nm. For GSSG measurement, deproteinated samples were first reduced with dithiothreitol (DTT, 10 mM, 15 min, room temperature).

For reactive oxygen species (ROS) production measurements, cell lysates (1:10 dilution) were combined with 100 µM 2′,7′-dichlorodihydrofluorescein diacetate (DCFH-DA) in DPBS according to Kim and Xue (2020). After dark incubation (37°C, 30 min), fluorescence was measured (excitation: 485 nm, emission: 530 nm) and normalized to total soluble protein content.

2.5 Statistical analysis

All statistical analyses were performed using GraphPad Prism version 10.3 (GraphPad Software, Inc., San Diego, CA, United States). Data are presented as mean ± standard deviation (SD). Statistical significance was set at $p < 0.05$. TEER measurements, paracellular permeability, and gene expression data were analyzed using one-way ANOVA followed by Tukey's *post hoc* test. Mucin quantification and dome count data were evaluated using two-way ANOVA followed by Šidák's multiple comparison test. Through Python's OpenCV library, dome structure comparisons (coverage, eccentricity, and contiguous objects) between static and dynamic conditions were analyzed by non-parametric Mann-Whitney U test at each time point. Cell viability, LDH release, redox status markers, and ROS measurements were analyzed using one-way ANOVA followed by Tukey's *post hoc* test.

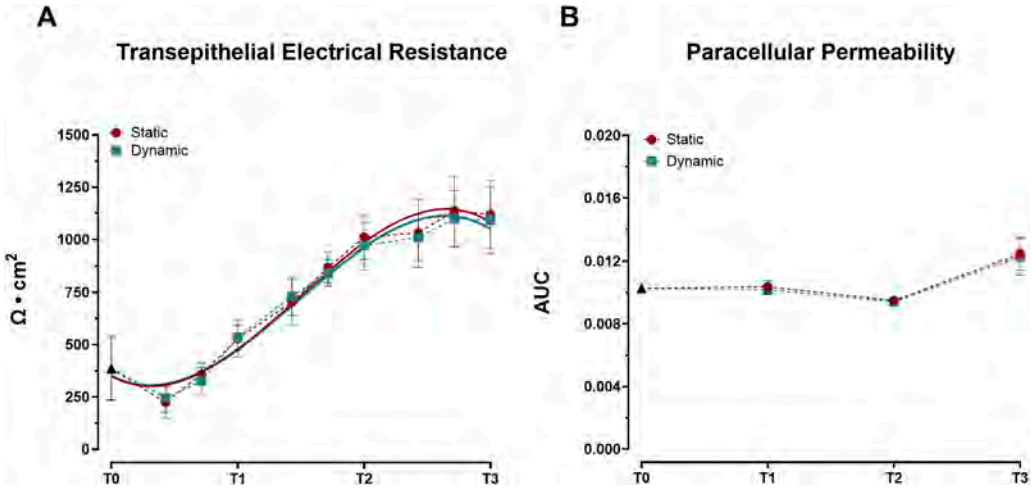

FIGURE 1
Development of barrier properties in Caco-2/HT29-MTX-E12 co-cultures under static and dynamic conditions during differentiation. **(A)** Transepithelial Electrical Resistance (TEER) measurements. Values were recorded at ten time points: 0 (T0), 3, 5, 7 (T1), 10, 12, 14 (T2), 17, 19, and 21 (T3) days post-confluence and expressed as $\Omega \times cm^2$. Lines represent third-order polynomial fits to the experimental values. Data points represent mean ± SD (n = 23–36 from three independent experiments). Statistical significance was assessed using one-way ANOVA followed by Tukey's *post hoc* test, with no significant differences between conditions. **(B)** Paracellular permeability assessed by phenol red transport, expressed as area under the curve (AUC) of transepithelial flux. Measurements were taken at four time points: immediately after reaching confluence (T0), and at 7 (T1), 14 (T2), and 21 (T3) days post-confluence. Data shown as mean ± SD (n = 4 from two independent experiments). Statistical significance was assessed using one-way ANOVA followed by Tukey's *post hoc* test. No significant differences were observed between static and dynamic conditions at each time point. Both conditions showed significantly increased permeability at T3 compared to earlier time points (T0, T1, and T2; $p < 0.05$).

3 Results

3.1 Dynamic culture conditions promote mucin production without affecting epithelial differentiation

Barrier integrity development, monitored through TEER measurements, showed progressive enhancement under both static and dynamic conditions throughout the 21-day culture period. TEER values exhibited consistent increases, reaching approximately 1,100 $\Omega \times cm^2$ by day 19 and stabilizing around 1,000 $\Omega \times cm^2$ by day 21 (Figure 1A). This pattern demonstrates successful establishment of the epithelial barrier through tight junctions by day 19, regardless of mechanical stimulation. In contrast to TEER measurements, paracellular permeability analysis revealed distinct temporal dynamics. While permeability remained comparable between static and dynamic conditions during early culture periods (T0–T2), both conditions showed a significant increase in permeability at T3 ($p < 0.05$ vs. T0, T1, and T2; Figure 1B).

Assessment of key intestinal differentiation markers revealed distinct temporal expression profiles between barrier-associated and secretory genes. Expression analysis of genes related to epithelial integrity and enterocyte function (*CDH1*, *TJP1*) (Figures 2A, B) and brush border enzymes (*ALPI*, *DPP4*, *SI*) (Figures 2C–E) demonstrated similar upward trends between static and dynamic conditions. The comparable expression levels of these markers establish that mechanical stimulation did not significantly alter the differentiation program of intestinal epithelial cells. However, mechanical stimulation markedly influenced goblet cell-specific genes. By day 21, cells cultured under dynamic conditions exhibited significant upregulation of both mucin genes, *MUC2* and *MUC5AC*, compared to static cultures (Figures 2F, G).

To confirm these transcriptional changes at the protein level, we quantified *in cellulo* mucin production throughout the differentiation period. While cytosolic mucin levels were initially comparable between conditions at day 7 (T1), dynamic cultures showed significantly higher concentrations by day 14 (T2), displaying more than two-fold increase compared to static conditions (Figure 3). Interestingly, this difference was not maintained at T3, where mucin levels were similar between conditions. This enhanced intracellular mucin content at T2 aligns with the gene expression data, though with a temporal offset.

3.2 Dynamic culture conditions enhance three-dimensional epithelial organization

Confocal microscopy analysis characterized the three-dimensional organization of the epithelial layer through sequential optical sections and 3D surface plot reconstructions (Figure 4). Images were acquired at 2 µm intervals from the Transwell membrane to the top of the cell multilayer under both static (Figures 4A–C) and dynamic (Figures 4E–G) conditions. WGA staining (green) labeled the mucus layer, while TO-PRO-3 (blue) marked cell nuclei, enabling visualization of the spatial distribution of cellular and mucus components, as previously described (García-Rodríguez et al., 2018). The WGA-stained mucus layer outlined the outer culture layer, facilitating accurate three-dimensional reconstruction of the epithelial architecture, as shown in the surface plots (Figures 4D, H).

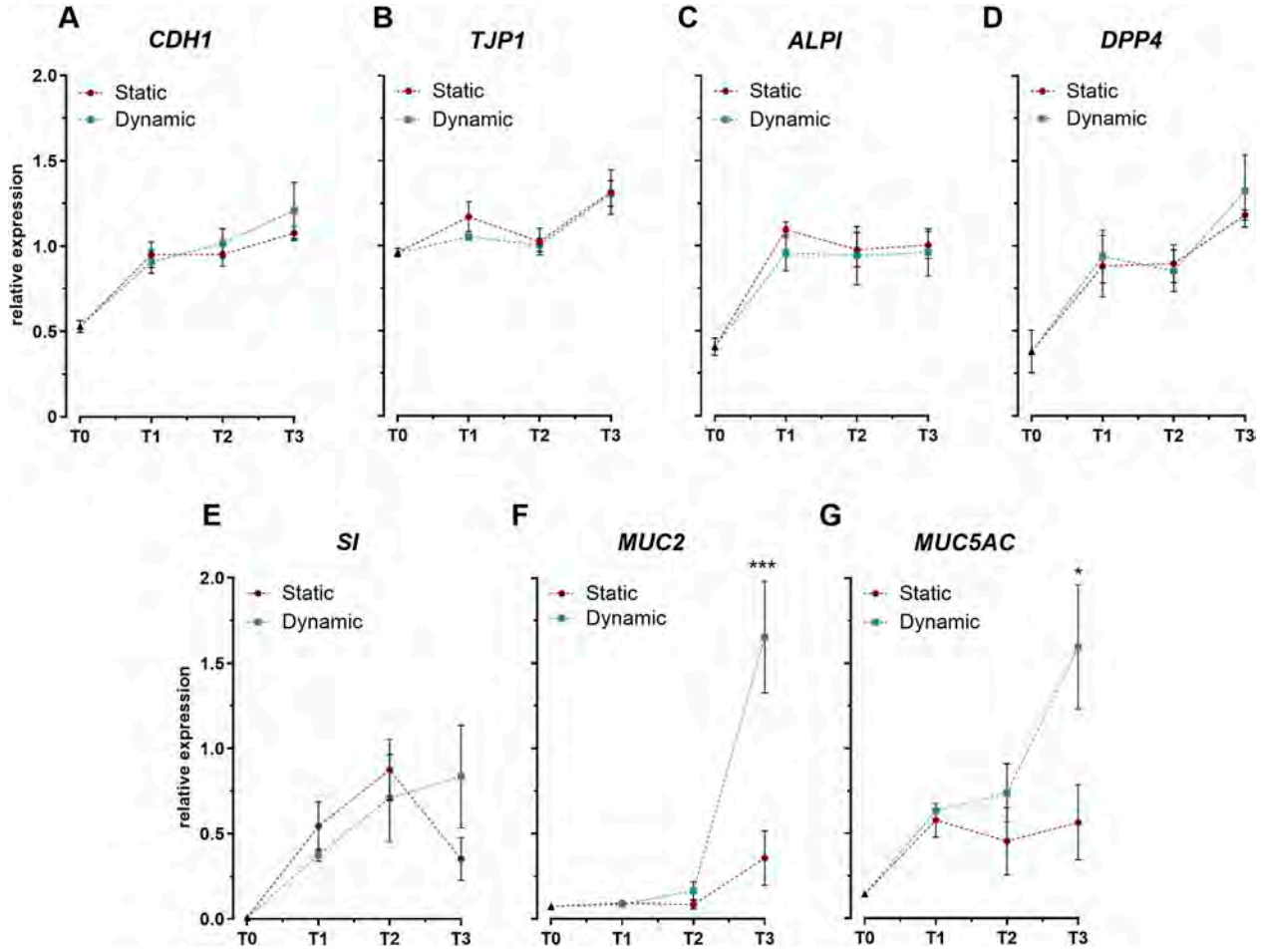

FIGURE 2
Expression profiles of key intestinal differentiation markers in Caco-2/HT29-MTX-E12 co-cultures under static and dynamic conditions. **(A–B)** Expression of genes encoding tight junction proteins: cadherin-1 (*CDH1*) and tight junction protein-1 (*TJP1*). **(C–E)** Expression of genes encoding brush border enzymes: intestinal alkaline phosphatase (*ALPI*), dipeptidyl peptidase-4 (*DPP4*), and sucrase-isomaltase (*SI*). **(F–G)** Expression of genes encoding mucins: mucin-2 (*MUC2*) and mucin-5AC (*MUC5AC*). Gene expression was analyzed at four time points: immediately after confluence (T0), and at 7 (T1), 14 (T2), and 21 (T3) days post-confluence. Data are expressed as relative expression values normalized to the geometric mean of *GAPDH* and *RPLP0* reference genes. Values represent mean ± SD from three biological replicates. Statistical significance between static and dynamic conditions at each time point was assessed using one-way ANOVA followed by Tukey's *post hoc* test ($^{*}p < 0.05$,$^{***}p < 0.001$).

Building on this imaging approach, detailed analysis revealed distinct patterns in the three-dimensional organization of the epithelial layer between static and dynamic conditions. Initial 3D surface plot reconstructions showed similar dome formation patterns across both conditions from T0 to T3 (Supplementary Figure S1), with no significant differences in dome counts (Figure 5). This led us to conduct a more detailed analysis using sequential optical sections (z-stacks) to examine three key parameters: cell coverage density, multicellular organization (through contiguous cellular structures), and geometric arrangement (via eccentricity measurements).

The z-stack analysis revealed progressive differences in epithelial organization between conditions (Figure 6). At T1, both conditions achieved similar initial monolayer formation, with 75%–90% surface coverage through the first 14 µm from the insert. However, by T2, distinct organizational patterns emerged. Dynamic cultures maintained approximately 80% cell coverage up to 14 µm height, with gradual decrease in higher sections, while static cultures showed steeper coverage reduction, reaching only around 50% at comparable heights. These differences became more pronounced at T3, where static cultures displayed a steeper decline in coverage in higher sections, falling below 20%.

The formation of three-dimensional epithelial structures also showed temporal evolution (Supplementary Figure S2). At T1, both conditions displayed minimal organization with only 2–3 contiguous structures present in the lower cell layers. By T2, dynamic conditions supported a more organized and cohesive formation of cellular structures in the intermediate layers, with approximately 10 objects. In contrast, static cultures showed significantly higher counts but with greater variability across sections. At T3, dynamic cultures established a stable epithelial architecture with 15–20 organized structures across the upper layers, whereas static cultures, although achieving

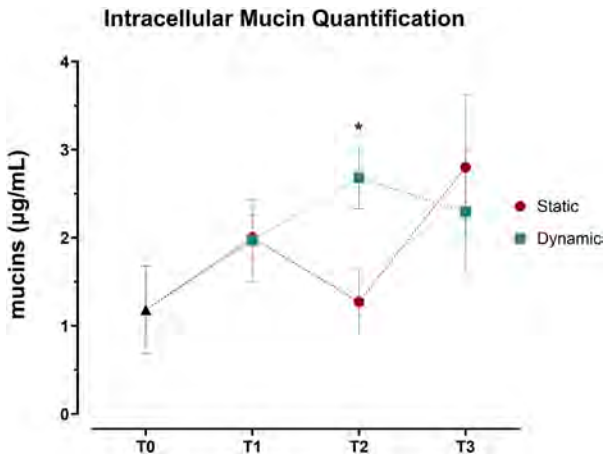

FIGURE 3
Quantification of intracellular mucins in Caco-2/HT29-MTX-E12 co-cultures under static and dynamic conditions. Intracellular mucin content, expressed as µg/mL, was measured using periodic acid-Schiff (PAS) assay at four time points: immediately after confluence (T0), and at 7 (T1), 14 (T2), and 21 (T3) days post-confluence. Values represent mean ± SD from four biological replicates across two independent experiments (n = 4). Statistical significance was assessed using two-way ANOVA followed by Šidák's multiple comparison test, with significant differences between static and dynamic conditions at T2 (*$p < 0.05$).

similar counts, exhibited less consistent organization in the upper regions (Supplementary Figure S3A).

Geometric analysis through eccentricity measurements revealed distinct temporal patterns (Supplementary Figure S3B). Initial structures showed low eccentricity values (0.2–0.4) in both conditions. At T2, eccentricity values in the lower sections under dynamic conditions were lower than those observed in static cultures, indicating a more rounded cell structure at the base. This difference diminished in the upper sections, where both static and dynamic conditions converged around higher eccentricity values (0.7–0.8). By T3, eccentricity profiles across sections for both conditions became more similar, though static cultures exhibited more variable values throughout the culture period.

3.3 Digested SMP maintains cell viability across multiple exposure ratios

Since the dynamic growth model demonstrated comparable or superior results to the static model, subsequent experimental supplementation with digested SMP with TiO_2 were conducted exclusively under dynamic conditions. To optimize the exposure protocol, it was first necessary to determine the optimal exposure ratio for digested SMP that would maintain cell viability while maximizing exposure to the digesta. The results shown in Supplementary Figure S4 illustrate the relative cell viability of the co-culture exposed to digested SMP at three dilution ratios: 1:3, 1:10, and 1:20. In comparison to the control cells, no significant reduction in cell viability was observed at any dilution, with viability remaining above 90% across all conditions. Based on these results, the 1:3 and 1:10 dilutions were selected for subsequent experiments supplementation of the co-culture dynamic model with digested SMP with TiO_2.

3.4 TiO_2-supplemented digesta induces concentration-dependent oxidative stress

ICP-OES analysis of the SMP digesta revealed a Ti concentration of 1.25 µg/mL. This concentration matched the expected theoretical value for 1% w/v TiO_2-supplemented SMP, accounting for the eight-fold dilution that occurs during the semi-dynamic *in vitro* digestion process. To investigate the biological impact of TiO_2 at this concentration, the digested samples were tested on the enhanced co-culture model at selected dilution ratios (1:3 and 1:10), evaluating cell viability, membrane integrity, and oxidative status biomarkers.

The results show that cell viability, reported in Supplementary Figure S5A, decreased significantly at the 1:3 dilution compared to the control, while no significant reduction was observed at the 1:10 dilution. Interestingly, LDH assay (Supplementary Figure S5B), which measures cell membrane damage, showed no significant differences between the control and treated cells at either concentration, establishing that the reduced viability at 1:3 dilution was not due to direct membrane damage.

To further characterize the mechanism of viability loss, we evaluated the oxidative status of the supplemented cell co-cultures. TBARS levels in the media, an indicator of lipid peroxidation, were significantly elevated at the 1:3 dilution (Supplementary Figure S5C), indicating increased oxidative damage, while the 1:10 dilution showed no significant change compared to the control. The 1:3 dilution also showed higher, though not statistically significant, ROS accumulation (Supplementary Figure S5D).

The assessment of antioxidant defenses revealed that glutathione (GSH) levels (Supplementary Figure S5E) decreased significantly at both concentrations, indicating a depletion of cellular antioxidant capacity. Moreover, the ratio of reduced (GSH) to oxidized (GSSG) glutathione significantly declined at the 1:3 dilution (Supplementary Figure S5F), further supporting the induction of oxidative stress under these conditions.

4 Discussion

4.1 Development of enhanced Caco-2/HT29-MTX-E12 co-culture

Our investigation revealed distinct patterns of epithelial development between static and dynamic culture conditions, with mechanical stimulation selectively enhancing specific aspects of cellular differentiation and organization. The most interesting differences we observed concerned dome formation at T2, which occurs through active transepithelial fluid transport and fluid entrapment between cells and the substrate (Lever, 1985). These structures, recognized as one of the hallmarks of advanced epithelial differentiation (Rotoli et al., 2002), were

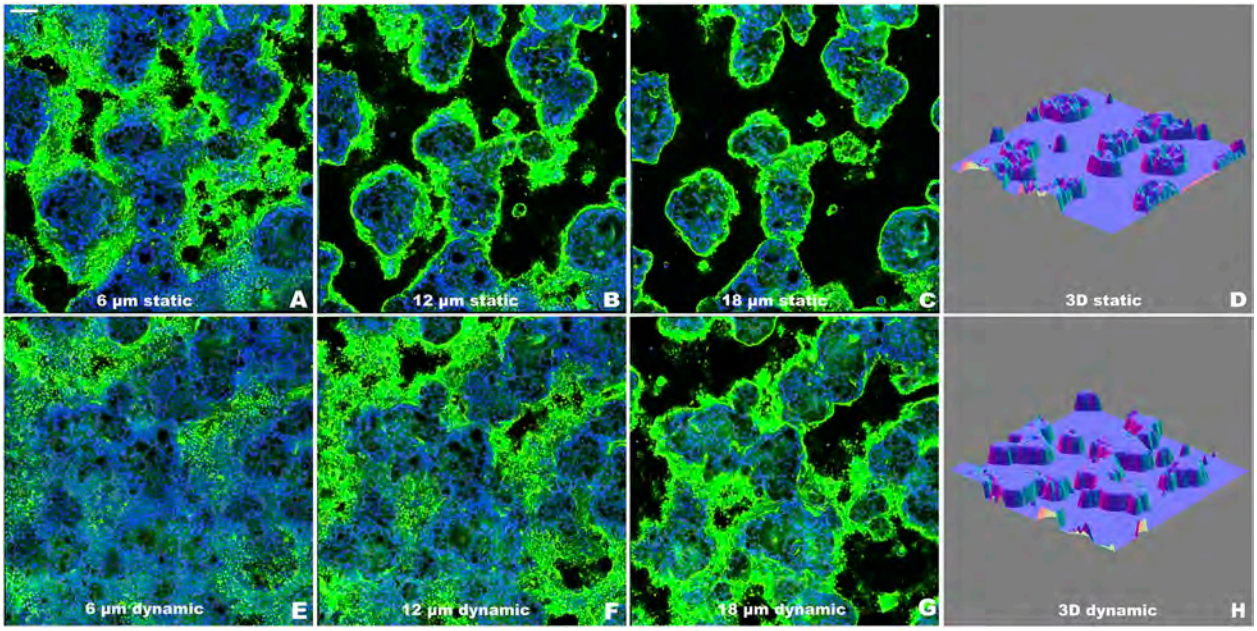

FIGURE 4
Evaluation of the epithelial organization of Caco-2/HT29-MTX-E12 co-culture using confocal microscopy at T2 as representative time point. **(A–C)** Representative optical sections along the *z*-axis under static conditions, acquired at increasing heights (6, 12, 18 µm) from the Transwell membrane. **(D)** 3D surface reconstruction of the complete z-stack from static condition. **(E–G)** Representative optical sections along the *z*-axis under dynamic conditions, acquired at increasing heights (6, 12, 18 µm) from the Transwell membrane. **(H)** 3D surface reconstruction of the complete z-stack from dynamic condition. Nuclei were stained with TO-PRO-3 (blue) and mucus layer was visualized using WGA (green). Images were acquired at day 14 (T2) post-confluence. Scale bar = 100 µm.

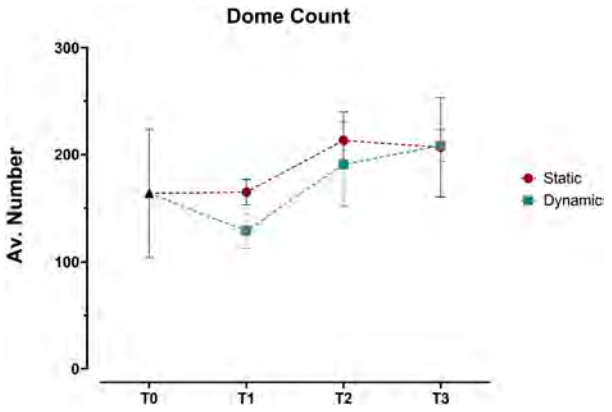

FIGURE 5
Quantification of dome structures in Caco-2/HT29-MTX-E12 co-cultures under static and dynamic conditions. Dome counts, expressed as average number of domes per angle view, were performed at four time points: immediately after confluence (T0), and at 7 (T1), 14 (T2), and 21 (T3) days post-confluence using 3D surface reconstructions from confocal z-stacks. Values represent mean ± SD from three technical replicates. Statistical significance was assessed using two-way ANOVA followed by Šidák's multiple comparison test, with no significant differences between static and dynamic conditions across all time points.

particularly prominent under dynamic conditions and maintained strong apical-basal polarity essential for nutrient transport and barrier function (Zweibaum et al., 2011).

When quantifying dome formation using 3D surface plots, we observed no significant differences between conditions, with dome numbers stabilizing around T3. This outcome contrasted with earlier observations by Hara et al. (1993), who reported a gradual increase in dome numbers plateauing around day 15. This discrepancy likely stems from methodological differences - our use of confocal microscopy for 3D analysis versus the bright-field imaging employed in earlier studies (Matsumoto et al., 1990; Hauck and Stanners, 1991; Herold et al., 1994), which could affect dome detection and quantification. Furthermore, the field lacks a standardized definition of what constitutes a "dome," contributing to variability in reporting and cross-study comparisons.

To address these methodological limitations, we developed a comprehensive analysis approach using confocal z-stacks that integrated cell coverage, eccentricity, and continuity parameters. This method revealed that dynamic conditions enhanced differentiation within a shorter timeframe, with distinct patterns in vertical organization. The mechanical forces specifically promoted cellular polarization processes, resulting in superior structural integrity and organization. Dynamic cultures progressed from early developmental stages reminiscent of initial epithelial formation (Fantini et al., 1986) to structures characteristic of differentiated intestinal epithelial monolayers (Ferraretto et al., 2018), maintaining stable organization with contiguous cell clusters.

Previous research established that domes typically appear around day 6 post-confluency, peak by day 15, and undergo fusion events that expand to cover larger portions of the monolayer (Pinto et al., 1983; Scaglione-Sewell et al., 1998). Our observations

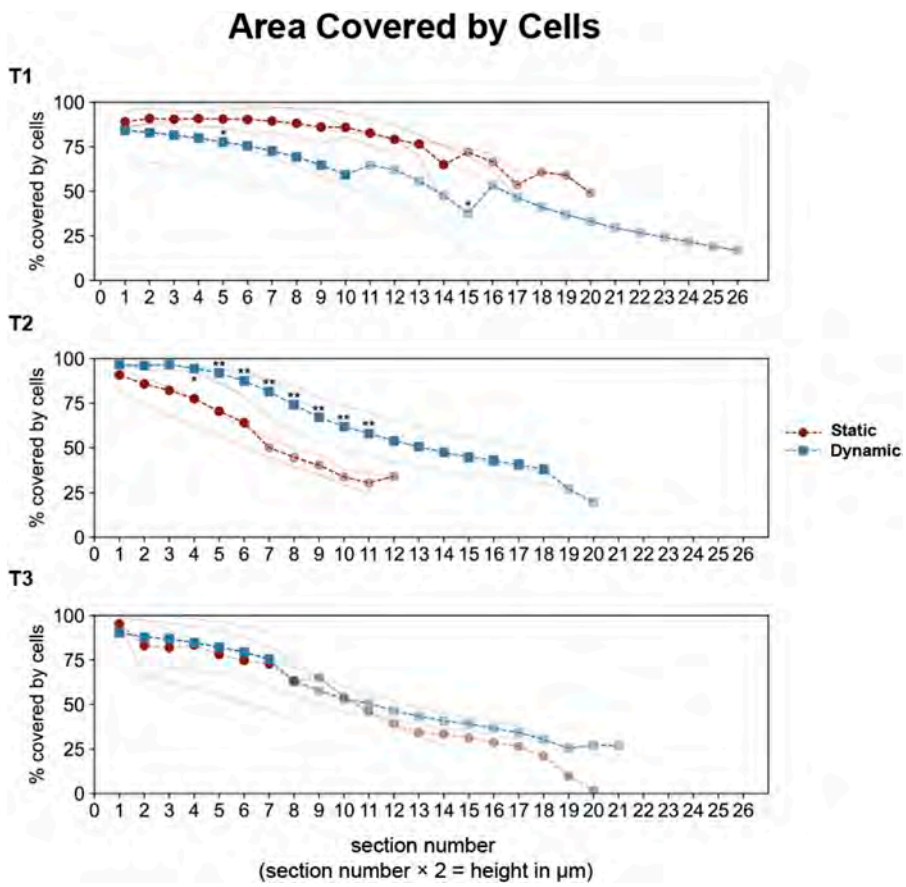

FIGURE 6
Quantitative analysis of epithelial coverage across optical sections in Caco-2/HT29-MTX-E12 co-cultures under static and dynamic conditions. Cell coverage was analyzed across sequential optical sections (2 µm intervals, sections 0–27 corresponding to heights 0–54 µm) at three time points: 7 (T1), 14 (T2), and 21 (T3) days post-confluence. Individual measurements from three technical replicates are shown as thin lines (red for static, blue for dynamic conditions). Dashed lines with markers represent full averages (circles for static, squares for dynamic), while partial averages (due to different cell scattering in optical sections) are shown with reduced opacity. Statistical significance between static and dynamic conditions was assessed using Mann-Whitney U test (*$p < 0.05$,**$p < 0.01$ for multiple comparisons), with significant differences ($p < 0.01$ for overall test across sections) observed at T2.

extended these findings, showing that mechanical forces not only accelerated dome formation but also enhanced their structural integration, promoting the fusion of smaller, circular domes into larger, more cohesive formations compared to static conditions.

The barrier function development, assessed through TEER measurements, showed an interesting pattern with no significant differences between static and dynamic conditions. This finding contrasts with previous studies where fluid shear stress upregulated tight junction proteins in both Caco-2 cells (Delon et al., 2019) and lung epithelial cells exposed to stretch-induced forces (Cavanaugh et al., 2001). The discrepancy between our co-culture results and previous monoculture studies demonstrates that the presence of mucus-producing HT29-MTX-E12 cells may modulate mechano-transduction pathways affecting tight junction assembly. The interaction between enterocytes and goblet cells likely introduces additional complexity to the mechanical regulation of barrier formation, potentially through paracrine signaling or altered mechanical force distribution across the heterogeneous epithelial layer.

An unexpected discrepancy emerged between barrier integrity measurements: while TEER values remained stable, indicating consistent ionic barrier function, paracellular permeability increased at T3 in both conditions, revealing a decline in size-selective barrier properties by the end of the time-course. This pattern mirrors *in vivo* observations of age-related increases in epithelial permeability, where tight junction function deteriorates over time (Salazar et al., 2023). The divergence between stable TEER values and increased permeability provides evidence of a distinct regulation of different transport pathways. While TEER primarily reflects paracellular resistance through tight junctions (Pongkorpsakol et al., 2021), permeability changes may reflect alterations in specific transport mechanisms or selective barrier properties (Horowitz et al., 2023). This differential response could result from two distinct mechanisms: the development of transcellular transport pathways and the selective modulation of specific tight junction proteins. The latter can regulate size-dependent permeability without affecting overall electrical resistance, as previously demonstrated for tight junction dynamics (Tervonen et al., 2019).

The mechanical stimulation's biological impact extended to cellular differentiation pathways, particularly affecting mucin production by goblet cells. While epithelial differentiation markers showed comparable expression levels between conditions, mucin-related genes displayed significant upregulation at T3 under dynamic conditions. This selective enhancement aligns with previous studies demonstrating positive effects of shear stress on goblet cell function (Reuter and Oelschlaeger, 2018; Lindner et al., 2021; Xu et al., 2021). The temporal dynamics showed distinct patterns between protein and gene expression levels. Increased intracellular mucin content was detected at T2, while peak mucin gene expression occurred later at T3. These observations reflect the complex dynamics of mucin synthesis, processing and secretion, where mucins undergo elaborate biosynthetic pathways including initial synthesis, dimerization, and extensive glycosylation (Asker et al., 1998; Thornton et al., 2008). The early accumulation of mucin content represents a regulatory response to mechanical forces, where initial mucin storage occurs independently of transcriptional changes (Perez-Vilar et al., 2006). The subsequent peak in mucin gene expression at T3 likely corresponds to active secretion of mature mucins into the extracellular space, resulting in depletion of intracellular stores (as shown from the PAS assay) despite elevated transcription (Dhanisha et al., 2018). However, it is important to note that our use of PAS assay alone may have limited our ability to detect acidic mucins. Future experiments will address this limitation by combining alcian blue and PAS staining as suggested by Harrop et al. (2012), allowing detection of both neutral and acidic mucins. Additionally, to obtain a complete picture of mucin dynamics, we will extend our analysis to include measurement of secreted mucins in the culture media.

The uncoupling between barrier integrity and mucin production revealed the complexity of cell differentiation under mechanical forces. As noted by Charras and Yap (2018), mechanical forces can strengthen specific cell-cell junctions without uniformly enhancing all barrier functions. This selective influence highlights how mechanical stimulation drives specialized responses—such as increased intracellular mucus accumulation—rather than broadly accelerating barrier formation.

4.2 Enhanced intestinal co-culture model application: a case study with TiO_2 nanoparticles in digested food matrix

Our initial evaluation using digested SMP demonstrated the model's robustness for food bioactivity and toxicology applications. The choice of SMP as a test matrix proved strategically valuable for several reasons. First, its relatively simple composition—primarily caseins and whey proteins—provided a controlled environment for assessing cellular responses without the confounding effects of complex food matrices (Mulet-Cabero et al., 2020). Second, the absence of bile salts and amylases in the digestion process minimized potential cytotoxic interference, allowing us to isolate the effects of protein digestion products on cellular viability (Kondrashina et al., 2024). The maintained cell viability across multiple dilutions of digested SMP (1:3 to 1:20) confirmed the model's compatibility with digested food products and established a reliable baseline for subsequent toxicological studies.

In this part of the study, we employed a low number of replicates in our exposure experiments due to the preliminary nature of the analysis, which was designed to test the co-culture model proposed. The primary aim of this paper is not an exhaustive toxicological assessment, but rather to establish a functional and physiologically relevant co-culture model of Caco-2 and HT29-MTX-E12 cells under the chosen conditions. Therefore, while the data provide important insights into the cellular responses to TiO_2-supplemented digesta, further studies with larger sample sizes will be necessary for a more robust evaluation of the effects.

Our investigation of TiO_2-supplemented digesta, while preliminary in nature with a limited number of replicates, provides valuable insights into the model's utility for nanotoxicology studies. Rather than aiming for an exhaustive toxicological assessment, these experiments served to prove our co-culture model's potential to detect and characterize cellular responses to food-relevant nanoparticle exposure. The observed responses to TiO_2 nanoparticles demonstrate clear concentration dependence and multiple stress pathways. At higher concentrations (1:3 dilution), decreased cell viability coincided with impaired mitochondrial function, consistent with previous findings (Huerta-García et al., 2014). The cellular internalization of TiO_2 nanoparticles, documented across various cell types (Freire et al., 2021), appears to trigger this cascade of cellular stress responses through mitochondrial dysfunction and subsequent oxidative damage.

Our results show a coordinated oxidative stress response characterized by increased lipid peroxidation and depleted antioxidant reserves. The significant elevation in TBARS levels, coupled with reduced GSH content and altered GSH/GSSG ratios at the 1:3 dilution, aligns with previous studies in intestinal models (Cao et al., 2020; Hoffmann et al., 2021). This oxidative stress signature represents a mechanism for TiO_2-induced cellular damage that could extend to DNA modification, as reported by Dorier et al. (2015). Notably, the preservation of membrane integrity, evidenced by stable LDH levels, despite significant oxidative stress markers, demonstrates that TiO_2 nanoparticles initially affect cellular metabolism rather than structural components. This finding, consistent with previous intestinal cell studies (Gerloff et al., 2012), point to a gradual progression of cellular dysfunction that might precede evident damage. The potential for TiO_2 nanoparticles to stimulate pro-inflammatory cytokine release (Lehotska Mikusova et al., 2023) further suggests that acute oxidative stress could evolve into chronic inflammatory responses.

The distinct temporal separation between early oxidative effects and potential long-term consequences emerges as a critical consideration for future research. While our model clearly detects acute cellular responses, the implications for chronic exposure scenarios, particularly regarding sustained oxidative stress and inflammatory signaling, require further investigation. This becomes especially relevant considering the widespread use of TiO_2 as a food additive and its potential for accumulation in intestinal tissues (Winkler et al., 2018).

5 Conclusion

Dynamic conditions established a physiologically representative epithelial barrier by T2, characterized by enhanced structural organization and cell-type specific functional development. The temporal coordination between morphological development and specialized cellular functions, particularly the mechanically-induced enhancement of goblet cell differentiation, demonstrates the importance of mechanical cues in establishing tissue-specific epithelial characteristics. This optimized co-culture model provides a practical balance between complexity and physiological relevance, making it particularly suitable for investigating food-related toxicology through its compatibility with digested materials. Our preliminary findings with TiO_2-supplemented digesta demonstrate the model's utility for nanotoxicology studies. Future experiments could explore the possibility of conducting toxicological assessments at day 14 of differentiation, potentially reducing experimental timelines while maintaining model reliability. This approach would bridge the gap between overly simplistic monocultures and complex 3D systems, offering a robust yet accessible platform for investigating epithelial barrier dynamics and food-matrix interactions.

Data availability statement

The datasets presented in this study can be found here: https://doi.org/10.5281/zenodo.14098875.

Author contributions

MS: Investigation, Software, Writing–original draft, Writing–review and editing, Data curation, Formal Analysis, Methodology. GP: Writing–original draft, Writing–review and editing, Investigation, Methodology. GL: Data curation, Formal Analysis, Methodology, Software, Writing–original draft, Writing–review and editing. MRR: Investigation, Writing–original draft, Writing–review and editing. MB: Conceptualization, Funding acquisition, Methodology, Resources, Writing–original draft, Writing–review and editing. LM: Conceptualization, Funding acquisition, Methodology, Resources, Writing–original draft, Writing–review and editing. FD: Conceptualization, Funding acquisition, Methodology, Resources, Writing–original draft, Writing–review and editing.

Funding

The author(s) declare that financial support was received for the research, authorship, and/or publication of this article. This work was supported by the University of Bologna "Alma Idea 2022" grant program (Line of Research B2-Sustainability, CUP: J33C22001420001) through the project 'GREENER' (How the complex physical-chemical and physiological events present in the human GastRointEstinal tract can intEract with NanomatERials potentially present in food: Journey from inorganic to biological using advanced *in vitro* models). GP was supported by a fellowship under this grant.

Acknowledgments

The authors gratefully acknowledge the valuable technical assistance of Andrea Simoni (Department of Agricultural and Food Sciences, University of Bologna, Italy) with ICP-OES analysis and Alberto Filetti (Department of Chemistry "Giacomo Ciamician", University of Bologna, Italy) with microscopy.

Conflict of interest

The authors declare that the research was conducted in the absence of any commercial or financial relationships that could be construed as a potential conflict of interest.

Generative AI statement

The authors declare that no Generative AI was used in the creation of this manuscript.

Publisher's note

Supplementary material

The Supplementary Material for this article can be found online at: https://www.frontiersin.org/articles/10.3389/fmolb.2024.1529027/full#supplementary-material

References

Antunes, F., Andrade, F., Araújo, F., Ferreira, D., and Sarmento, B. (2013). Establishment of a triple co-culture *in vitro* cell models to study intestinal absorption of peptide drugs. *Eur. J. Pharm. Biopharm.* 83, 427–435. doi:10.1016/j.ejpb.2012.10.003

Asker, N., Axelsson, M. A., Olofsson, S. O., and Hansson, G. C. (1998). Dimerization of the human MUC2 mucin in the endoplasmic reticulum is followed by a N-glycosylation-dependent transfer of the mono- and dimers to the Golgi apparatus. *J. Biol. Chem.* 273, 18857–18863. doi:10.1074/jbc.273.30.18857

Atallah, N., Deracinois, B., Boulier, A., Baniel, A., Jouan-Rimbaud Bouveresse, D., Ravallec, R., et al. (2020). *In vitro* assessment of the impact of industrial processes on the gastrointestinal digestion of milk protein matrices using the INFOGEST protocol. *Foods* 9, 1580. doi:10.3390/foods9111580

Baptista, L. S., Porrini, C., Kronemberger, G. S., Kelly, D. J., and Perrault, C. M. (2022). 3D organ-on-a-chip: the convergence of microphysiological systems and organoids. *Front. Cell Dev. Biol.* 10, 1043117. doi:10.3389/fcell.2022.1043117

Basson, M. D., Emenaker, N. J., and Hong, F. (1998). Differential modulation of human (Caco-2) colon cancer cell line phenotype by short chain fatty acids. *Proc. Soc. Exp. Biol. Med.* 217, 476–483. doi:10.3181/00379727-217-44261

Behrens, I., Stenberg, P., Artursson, P., and Kissel, T. (2001). Transport of lipophilic drug molecules in a new mucus-secreting cell culture model based on HT29-MTX cells. *Pharm. Res.* 18, 1138–1145. doi:10.1023/a:1010974909998

Bettini, S., Boutet-Robinet, E., Cartier, C., Comera, C., Gaultier, E., Dupuy, J., et al. (2017). Food-grade TiO_2 impairs intestinal and systemic immune homeostasis, initiates preneoplastic lesions and promotes aberrant crypt development in the rat colon. *Sci. Rep.* 7, 40373. doi:10.1038/srep40373

Bohets, H., Annaert, P., Mannens, G., Van Beijsterveldt, L., Anciaux, K., Verboven, P., et al. (2001). Strategies for absorption screening in drug discovery and development. *Curr. Top. Med. Chem.* 1, 367–383. doi:10.2174/1568026013394886

Boutillier, S., Fourmentin, S., and Laperche, B. (2022). History of titanium dioxide regulation as a food additive: a review. *Environ. Chem. Lett.* 20, 1017–1033. doi:10.1007/s10311-021-01360-2

Cao, X., Zhang, T., DeLoid, G. M., Gaffrey, M. J., Weitz, K. K., Thrall, B. D., et al. (2020). Evaluation of the cytotoxic and cellular proteome impacts of food-grade TiO_2 (E171) using simulated gastrointestinal digestions and a tri-culture small intestinal epithelial model. *NanoImpact* 17, 100202. doi:10.1016/j.impact.2019.100202

Cavanaugh, K. J., Oswari, J., and Margulies, S. S. (2001). Role of stretch on tight junction structure in alveolar epithelial cells. *Am. J. Respir. Cell Mol. Biol.* 25, 584–591. doi:10.1165/ajrcmb.25.5.4486

Charras, G., and Yap, A. S. (2018). Tensile forces and mechanotransduction at cell-cell junctions. *Curr. Biol.* 28, R445–R457. doi:10.1016/j.cub.2018.02.003

Dardik, A., Chen, L., Frattini, J., Asada, H., Aziz, F., Kudo, F. A., et al. (2005). Differential effects of orbital and laminar shear stress on endothelial cells. *J. Vasc. Surg.* 41, 869–880. doi:10.1016/j.jvs.2005.01.020

Delon, L. C., Guo, Z., Oszmiana, A., Chien, C. C., Gibson, R., Prestidge, C., et al. (2019). A systematic investigation of the effect of the fluid shear stress on Caco-2 cells towards the optimization of epithelial organ-on-chip models. *Biomaterials* 225, 119521. doi:10.1016/j.biomaterials.2019.119521

Dhanisha, S. S., Guruvayoorappan, C., Drishya, S., and Abeesh, P. (2018). Mucins: structural diversity, biosynthesis, its role in pathogenesis and as possible therapeutic targets. *Crit. Rev. Oncol. Hematol.* 122, 98–122. doi:10.1016/j.critrevonc.2017.12.006

Dharmani, P., Srivastava, V., Kissoon-Singh, V., and Chadee, K. (2009). Role of intestinal mucins in innate host defense mechanisms against pathogens. *J. Innate Immun.* 1, 123–135. doi:10.1159/000163037

Dorier, M., Brun, E., Veronesi, G., Barreau, F., Pernet-Gallay, K., Desvergne, C., et al. (2015). Impact of anatase and rutile titanium dioxide nanoparticles on uptake carriers and efflux pumps in Caco-2 gut epithelial cells. *Nanoscale* 7, 7352–7360. doi:10.1039/c5nr00505a

EFSA Panel on Food Additives and Flavourings (FAF), Younes, M., Aquilina, G., Castle, L., Engel, K. H., Fowler, P., Fürst, P., et al. (2021). Safety assessment of titanium dioxide (E171) as a food additive. *EFSA J.* 19, e06585. doi:10.2903/j.efsa.2021.6585

Fantini, J., Abadie, B., Tirard, A., Remy, L., Ripert, J. P., el Battari, A., et al. (1986). Spontaneous and induced dome formation by two clonal cell populations derived from a human adenocarcinoma cell line, HT29. *J. Cell Sci.* 83, 235–249. doi:10.1242/jcs.83.1.235

Faria, M. A., Melo, A., and Ferreira, I. (2020). Influence of dietary patterns on contaminants bioaccessibility and intestinal transport by *in vitro* assays. *Food Res. Int.* 137, 109358. doi:10.1016/j.foodres.2020.109358

FDA (Food and Drugs Administration) (2024). Titanium dioxide as a color additive in foods. Available at: https://www.fda.gov/industry/color-additives/titanium-dioxide-color-additive-foods (Accessed November 1, 2024).

Ferraretto, A., Bottani, M., De Luca, P., Cornaghi, L., Arnaboldi, F., Maggioni, M., et al. (2018). Morphofunctional properties of a differentiated Caco2/HT-29 co-culture as an *in vitro* model of human intestinal epithelium. *Biosci. Rep.* 38, BSR20171497. doi:10.1042/bsr20171497

Ferraretto, A., Gravaghi, C., Donetti, E., Cosentino, S., Donida, B. M., Bedoni, M., et al. (2007). New methodological approach to induce a differentiation phenotype in Caco-2 cells prior to post-confluence stage. *Anticancer Res.* 27, 3919–3925.

Ferruzza, S., Scarino, M. L., Gambling, L., Natella, F., and Sambuy, Y. (2003). Biphasic effect of iron on human intestinal Caco-2 cells: early effect on tight junction permeability with delayed onset of oxidative cytotoxic damage. *Cell Mol. Biol.* 49, 89–99.

Freire, K., Ordóñez Ramos, F., Soria, D. B., Pabón Gelves, E., and Di Virgilio, A. L. (2021). Cytotoxicity and DNA damage evaluation of TiO_2 and ZnO nanoparticles. Uptake in lung cells in culture. *Toxicol. Res.* 10, 192–202. doi:10.1093/toxres/tfaa112

Frohlich, E., and Roblegg, E. (2012). Models for oral uptake of nanoparticles in consumer products. *Toxicology* 291, 10–17. doi:10.1016/j.tox.2011.11.004

García-Rodríguez, A., Vila, L., Cortés, C., Hernández, A., and Marcos, R. (2018). Exploring the usefulness of the complex *in vitro* intestinal epithelial model Caco-2/HT29/Raji-B in nanotoxicology. *Food Chem. Toxicol.* 113, 162–170. doi:10.1016/j.fct.2018.01.042

Gerloff, K., Fenoglio, I., Carella, E., Kolling, J., Albrecht, C., Boots, A. W., et al. (2012). Distinctive toxicity of TiO_2 rutile/anatase mixed phase nanoparticles on Caco-2 cells. *Chem. Res. Toxicol.* 25, 646–655. doi:10.1021/tx200334k

Giromini, C., Lovegrove, J. A., Givens, D. I., Rebucci, R., Pinotti, L., Maffioli, E., et al. (2019). *In vitro*-digested milk proteins: evaluation of angiotensin-1-converting enzyme inhibitory and antioxidant activities, peptidomic profile, and mucin gene expression in HT29-MTX cells. *J. Dairy Sci.* 102, 10760–10771. doi:10.3168/jds.2019-16833

Guo, P., Weinstein, A. M., and Weinbaum, S. (2000). A hydrodynamic mechanosensory hypothesis for brush border microvilli. *Am. J. Physiol. Ren. Physiol.* 279, F698–F712. doi:10.1152/ajprenal.2000.279.4.F698

Hara, A., Hibi, T., Yoshioka, M., Toda, K., Watanabe, N., Hayashi, A., et al. (1993). Changes of proliferative activity and phenotypes in spontaneous differentiation of a colon cancer cell line. *Jpn. J. Cancer Res.* 84, 625–632. doi:10.1111/j.1349-7006.1993.tb02022.x

Hardy, J. G., Davis, S. S., and Wilson, C. G. (1989). *Drug delivery to the gastrointestinal tract*. Chichester, England: Ellis Horwood.

Harrop, C. A., Thornton, D. J., and McGuckin, M. A. (2012). Detecting, visualising, and quantifying mucins. *Methods Mol. Biol.* 842, 49–66. doi:10.1007/978-1-61779-513-8_3

Hauck, W., and Stanners, C. P. (1991). Control of carcinoembryonic antigen gene family expression in a differentiating colon-carcinoma cell-line, Caco-2. *Cancer Res.* 51, 3526–3533.

Heringa, M. B., Peters, R. J. B., Bleys, R., van der Lee, M. K., Tromp, P. C., van Kesteren, P. C. E., et al. (2018). Detection of titanium particles in human liver and spleen and possible health implications. *Part Fibre Toxicol.* 15, 15. doi:10.1186/s12989-018-0251-7

Herold, G., Rogler, G., Rogler, D., and Stange, E. F. (1994). Morphology of CaCo-2 cells varies in different cell batches. *Vitro Cell Dev Biol Anim* 30, 289–291. doi:10.1007/BF02631447

Hiebl, V., Schachner, D., Ladurner, A., Heiss, E. H., Stangl, H., and Dirsch, V. M. (2020). Caco-2 cells for measuring intestinal cholesterol transport - possibilities and limitations. *Biol. Proced. Online* 22, 7. doi:10.1186/s12575-020-00120-w

Hoffmann, P., Burmester, M., Langeheine, M., Brehm, R., Empl, M. T., Seeger, B., et al. (2021). Caco-2/HT29-MTX co-cultured cells as a model for studying physiological properties and toxin-induced effects on intestinal cells. *PLoS One* 16, e0257824. doi:10.1371/journal.pone.0257824

Horowitz, A., Chanez-Paredes, S. D., Haest, X., and Turner, J. R. (2023). Paracellular permeability and tight junction regulation in gut health and disease. *Nat. Rev. Gastroenterol. Hepatol.* 20, 417–432. doi:10.1038/s41575-023-00766-3

Huerta-García, E., Pérez-Arizti, J. A., Márquez-Ramírez, S. G., Delgado-Buenrostro, N. L., Chirino, Y. I., Gutiérrez Iglesias, G., et al. (2014). Titanium dioxide nanoparticles induce strong oxidative stress and mitochondrial damage in glial cells. *Free Radic. Biol. Med.* 73, 84–94. doi:10.1016/j.freeradbiomed.2014.04.026

JECFA (2023). "Ninety-sixth meeting - Joint FAO/WHO Expert committee on food additives (JECFA)," in *Safety evaluation of certain food additives and contaminants* (Geneva: World Health Organization).

Jensen, K. A., Kembouche, Y., Christiansen, E., Jacobsen, N., Wallin, H., Guiot, C., et al. (2011). "Final protocol for producing suitable manufactured nanomaterial exposure media," in *The NANOGENOTOX Joint action: safety evaluation of manufactured nanomaterials*. Editor K. A. Jensen (Copenhagen: National Research Centre for the Working Environment), 1–87.

Jiang, L. F., Long, X. W., and Meng, Q. (2013). Rhamnolipids enhance epithelial permeability in Caco-2 monolayers. *Int. J. Pharm.* 446, 130–135. doi:10.1016/j.ijpharm.2013.02.003

Johansson, M. E. V., and Hansson, G. C. (2016). Immunological aspects of intestinal mucus and mucins. *Nat. Rev. Immunol.* 16, 639–649. doi:10.1038/nri.2016.88

Kilcoyne, M., Gerlach, J. Q., Farrell, M. P., Bhavanandan, V. P., and Joshi, L. (2011). Periodic acid-Schiff's reagent assay for carbohydrates in a microtiter plate format. *Anal. Biochem.* 416, 18–26. doi:10.1016/j.ab.2011.05.006

Kim, H., and Xue, X. (2020). Detection of total reactive oxygen species in adherent cells by 2',7'-dichlorodihydrofluorescein diacetate staining. *J. Vis. Exp.*, e60682. doi:10.3791/60682

Koeneman, B. A., Zhang, Y., Hristovski, K., Westerhoff, P., Chen, Y., Crittenden, J. C., et al. (2009). Experimental approach for an *in vitro* toxicity assay with non-aggregated quantum dots. *Toxicol Vitro* 23, 955–962. doi:10.1016/j.tiv.2009.05.007

Kondrashina, A., Arranz, E., Cilla, A., Faria, M. A., Santos-Hernández, M., Miralles, B., et al. (2024). Coupling *in vitro* food digestion with *in vitro* epithelial absorption; recommendations for biocompatibility. *Crit. Rev. Food Sci. Nutr.* 64, 9618–9636. doi:10.1080/10408398.2023.2214628

Lechner, J., Hekl, D., Gatt, H., Voelp, M., and Seppi, T. (2011). Monitoring of the dynamics of epithelial dome formation using a novel culture chamber for long-term continuous live-cell imaging. *Methods Mol. Biol.* 763, 169–178. doi:10.1007/978-1-61779-191-8_11

Lehotska Mikusova, M., Busova, M., Tulinska, J., Masanova, V., Liskova, A., Uhnakova, I., et al. (2023). Titanium dioxide nanoparticles modulate systemic immune response and increase levels of reduced glutathione in mice after seven-week inhalation. *Nanomater. (Basel)* 13, 767. doi:10.3390/nano13040767

Lesuffleur, T., Porchet, N., Aubert, J. P., Swallow, D., Gum, J. R., Kim, Y. S., et al. (1993). Differential expression of the human mucin genes MUC1 to MUC5 in relation to growth and differentiation of different mucus-secreting HT-29 cell subpopulations. *J. Cell Sci.* 106, 771–783. doi:10.1242/jcs.106.3.771

Lever, J. E. (1985). "Inducers of dome formation in epithelial cell cultures including agents that cause differentiation," in *Tissue culture of epithelial cells*. Editor M. Taub (Boston, MA: Springer US), 3–22.

Liang, E., Chessic, K., and Yazdanian, M. (2000). Evaluation of an accelerated Caco-2 cell permeability model. *J. Pharm. Sci.* 89, 336–345. doi:10.1002/(SICI)1520-6017(200003)89:3<336::AID-JPS5>3.0.CO;2-M

Lindner, M., Laporte, A., Block, S., Elomaa, L., and Weinhart, M. (2021). Physiological shear stress enhances differentiation, mucus-formation and structural 3D organization of intestinal epithelial cells *in vitro*. *Cells* 10, 2062. doi:10.3390/cells10082062

Liu, P., Tu, J., Wang, W., Li, Z., Li, Y., Yu, X., et al. (2022). Effects of mechanical stress stimulation on function and expression mechanism of osteoblasts. *Front. Bioeng. Biotechnol.* 10, 830722. doi:10.3389/fbioe.2022.830722

Mantle, M., and Allen, A. (1978). A colorimetric assay for glycoproteins based on the periodic acid/Schiff stain. *Biochem. Soc. Trans.* 6, 607–609. doi:10.1042/bst0060607

Martínez-Maqueda, D., Miralles, B., and Recio, I. (2015). "HT29 cell line," in *The Impact of Food Bioactives on Health: in vitro and ex vivo models*. Editors K. Verhoeckx, P. Cotter, I. López-Expósito, C. Kleiveland, T. Lea, A. Mackie, et al. (Cham: Springer), 113–124.

Matsumoto, H., Erickson, R. H., Gum, J. R., Yoshioka, M., Gum, E., and Kim, Y. S. (1990). Biosynthesis of alkaline phosphatase during differentiation of the human colon cancer cell line Caco-2. *Gastroenterology* 98, 1199–1207. doi:10.1016/0016-5085(90)90334-w

McCracken, C., Zane, A., Knight, D. A., Dutta, P. K., and Waldman, W. J. (2013). Minimal intestinal epithelial cell toxicity in response to short- and long-term food-relevant inorganic nanoparticle exposure. *Chem. Res. Toxicol.* 26, 1514–1525. doi:10.1021/tx400231u

Miner-Williams, W., Moughan, P. J., and Fuller, M. F. (2009). Methods for mucin analysis: a comparative study. *J. Agric. Food Chem.* 57, 6029–6035. doi:10.1021/jf901036r

Mulet-Cabero, A. I., Egger, L., Portmann, R., Menard, O., Marze, S., Minekus, M., et al. (2020). A standardised semi-dynamic *in vitro* digestion method suitable for food - an international consensus. *Food Funct.* 11, 1702–1720. doi:10.1039/c9fo01293a

Paone, P., and Cani, P. D. (2020). Mucus barrier, mucins and gut microbiota: the expected slimy partners? *Gut* 69, 2232–2243. doi:10.1136/gutjnl-2020-322260

Pereira, C., Costa, J., Sarmento, B., and Araújo, F. (2016). "Cell-based *in vitro* models for intestinal permeability studies," in *Concepts and Models for drug permeability studies*. Editor B. Sarmento (Elsevier Science), 57–81.

Perez-Vilar, J., Mabolo, R., McVaugh, C. T., Bertozzi, C. R., and Boucher, R. C. (2006). Mucin granule intraluminal organization in living mucous/goblet cells. Roles of protein post-translational modifications and secretion. *J. Biol. Chem.* 281, 4844–4855. doi:10.1074/jbc.M510520200

Peters, R. J., van Bemmel, G., Herrera-Rivera, Z., Helsper, H. P., Marvin, H. J., Weigel, S., et al. (2014). Characterization of titanium dioxide nanoparticles in food products: analytical methods to define nanoparticles. *J. Agric. Food Chem.* 62, 6285–6293. doi:10.1021/jf5011885

Pinto, M., Robine-Leon, S., Appay, M. D., Kedinger, M., Triadou, N., Dussaulx, E., et al. (1983). Enterocyte-like differentiation and polarization of the human colon carcinoma cell line Caco-2 in culture. *Biol. Cell* 47, 323–330.

Pongkorpsakol, P., Satianrapapong, W., Wongkrasant, P., Steinhagen, P. R., Tuangkijkul, N., Pathomthongtaweechai, N., et al. (2021). Establishment of intestinal epithelial cell monolayers and their use in calcium switch assay for assessment of intestinal tight junction assembly. *Methods Mol. Biol.* 2367, 273–290. doi:10.1007/7651_2021_347

Potter, T. M., Neun, B. W., and Stern, S. T. (2011). Assay to detect lipid peroxidation upon exposure to nanoparticles. *Methods Mol. Biol.* 697, 181–189. doi:10.1007/978-1-60327-198-1_19

Reuter, C., and Oelschlaeger, T. A. (2018). Enhancement of mucus production in eukaryotic cells and quantification of adherent mucus by ELISA. *Bio Protoc.* 8, e2879. doi:10.21769/BioProtoc.2879

Rompelberg, C., Heringa, M. B., van Donkersgoed, G., Drijvers, J., Roos, A., Westenbrink, S., et al. (2016). Oral intake of added titanium dioxide and its nanofraction from food products, food supplements and toothpaste by the Dutch population. *Nanotoxicology* 10, 1404–1414. doi:10.1080/17435390.2016.1222457

Ropers, M. H., Terrisse, H., Mercier-Bonin, M., and Humbert, B. (2017). "Titanium dioxide as food additive," in *Food applications of titanium dioxide*. Editors A. M. Grumezescu, and A. M. Holban (London: Academic Press), 3–21.

Rotoli, B. M., Orlandini, G., Gatti, R., Dall'Asta, V., Gazzola, G. C., and Bussolati, O. (2002). Employment of confocal microscopy for the dynamic visualization of domes in intact epithelial cell cultures. *Cells Tissues Organs* 170, 237–245. doi:10.1159/000047927

Salazar, A. M., Aparicio, R., Clark, R. I., Rera, M., and Walker, D. W. (2023). Intestinal barrier dysfunction: an evolutionarily conserved hallmark of aging. *Dis. Model Mech.* 16, dmm049969. doi:10.1242/dmm.049969

Sambuy, Y., De Angelis, I., Ranaldi, G., Scarino, M. L., Stammati, A., and Zucco, F. (2005). The Caco-2 cell line as a model of the intestinal barrier: influence of cell and culture-related factors on Caco-2 cell functional characteristics. *Cell Biol. Toxicol.* 21, 1–26. doi:10.1007/s10565-005-0085-6

Scaglione-Sewell, B., Abraham, C., Bissonnette, M., Skarosi, S. F., Hart, J., Davidson, N. O., et al. (1998). Decreased PKC-alpha expression increases cellular proliferation, decreases differentiation, and enhances the transformed phenotype of CaCo-2 cells. *Cancer Res.* 58, 1074–1081.

Schindelin, J., Arganda-Carreras, I., Frise, E., Kaynig, V., Longair, M., Pietzsch, T., et al. (2012). Fiji: an open-source platform for biological-image analysis. *Nat. Methods* 9, 676–682. doi:10.1038/nmeth.2019

Segeritz, C. P., and Vallier, L. (2017). "Cell culture," in *Basic science methods for clinical researchers*. Editor M. Jalali (London: Academic Press), 151–172.

Smetanová, L., Stětinová, V., Svoboda, Z., and Kvetina, J. (2011). Caco-2 cells, biopharmaceutics classification system (BCS) and biowaiter. *Acta Medica (Hradec Kralove)* 54, 3–8. doi:10.14712/18059694.2016.9

Song, C., Chai, Z., Chen, S., Zhang, H., Zhang, X., and Zhou, Y. (2023). Intestinal mucus components and secretion mechanisms: what we do and do not know. *Exp. Mol. Med.* 55, 681–691. doi:10.1038/s12276-023-00960-y

Tervonen, A., Ihalainen, T. O., Nymark, S., and Hyttinen, J. (2019). Structural dynamics of tight junctions modulate the properties of the epithelial barrier. *PLoS One* 14, e0214876. doi:10.1371/journal.pone.0214876

Thornton, D. J., Rousseau, K., and McGuckin, M. A. (2008). Structure and function of the polymeric mucins in airways mucus. *Annu. Rev. Physiol.* 70, 459–486. doi:10.1146/annurev.physiol.70.113006.100702

Vandesompele, J., De Preter, K., Pattyn, F., Poppe, B., Van Roy, N., De Paepe, A., et al. (2002). Accurate normalization of real-time quantitative RT-PCR data by geometric averaging of multiple internal control genes. *Genome Biol.* 3, research0034.0031. doi:10.1186/gb-2002-3-7-research0034

Vieira, A., Gramacho, A., Rolo, D., Vital, N., Silva, M. J., and Louro, H. (2022). Cellular and molecular mechanisms of toxicity of ingested titanium dioxide nanomaterials. *Adv. Exp. Med. Biol.* 1357, 225–257. doi:10.1007/978-3-030-88071-2_10

Vuolo, M. M., da Silva-Maia, J. K., and Batista, Â. G. (2022). "The GSH colorimetric method as measurement of antioxidant status in serum and rodent tissues," in *Basic protocols in foods and nutrition*. Editor C. B. Betim Cazarin (New York: Humana Press), 187–194.

Wang, J. X., Zhou, G. Q., Chen, C. Y., Yu, H. W., Wang, T. C., Ma, Y. M., et al. (2007). Acute toxicity and biodistribution of different sized titanium dioxide particles in mice after oral administration. *Toxicol. Lett.* 168, 176–185. doi:10.1016/j.toxlet.2006.12.001

Weir, A., Westerhoff, P., Fabricius, L., Hristovski, K., and von Goetz, N. (2012). Titanium dioxide nanoparticles in food and personal care products. *Environ. Sci. Technol.* 46, 2242–2250. doi:10.1021/es204168d

Welcome, M. O. (2018). "Cellular organization of the gastrointestinal tract," in *Gastrointestinal physiology: development, principles and mechanisms of regulation* (Cham: Springer), 107–199.

Willemsen, L. E., Koetsier, M. A., van Deventer, S. J., and van Tol, E. A. (2003). Short chain fatty acids stimulate epithelial mucin 2 expression through differential effects on prostaglandin E_1 and E_2 production by intestinal myofibroblasts. *Gut* 52, 1442–1447. doi:10.1136/gut.52.10.1442

Winkler, H. C., Notter, T., Meyer, U., and Naegeli, H. (2018). Critical review of the safety assessment of titanium dioxide additives in food. *J. Nanobiotechnology* 16, 51. doi:10.1186/s12951-018-0376-8

Xu, Y., Bai, T., Xiong, Y., Liu, C., Liu, Y., Hou, X., et al. (2021). Mechanical stimulation activates Piezo1 to promote mucin2 expression in goblet cells. *J. Gastroenterol. Hepatol.* 36, 3127–3139. doi:10.1111/jgh.15596

Yamabayashi, S. (1987). Periodic acid — Schiff — alcian Blue: a method for the differential staining of glycoproteins. *Histochem J.* 19, 565–571. doi:10.1007/Bf01687364

Zweibaum, A., Laburthe, M., Grasset, E., and Louvard, D. (2011). "Use of cultured cell lines in studies of intestinal cell differentiation and function," in *Comprehensive physiology*. Editor R. Terjung (Hoboken: John Wiley and Sons), 223–255.